11th World Congress on Computational Mechanics (WCCM XI)
5th European Conference on Computational Mechanics (ECCM V)
6th European Conference on Computational Fluid Dynamics (ECFD VI)
E. Oñate, J. Oliver and A. Huerta (Eds)

A NUMERICAL INVESTIGATION OF SCRAMJET ENGINE AIR INTAKES FOR THE 14-X HYPERSONIC VEHICLE

AUGUSTO F. MOURA*, MAURÍCIO A. P. ROSA*

* Instituto de Estudos Avançados (IEAv)
Departamento de Ciência e Tecnologia Aeroespacial
Trevo Cel. Aviador José Alberto Albano do Amarante, 1, 12.228-001, São José dos Campos, Brasil
e-mail: augustofontan@gmail.com, www.ieav.cta.br

Key Words: *hypersonic flow, scramjet intake, performance parameters*

Abstract. This work is part of the research and development, at the Institute for Advanced Studies (IEAv), of the first Brazilian hypersonic vehicle prototype, the 14-X airplane. It presents CFD results and performance calculations of the air intake section of some scramjet engine configurations under several operating conditions assuming 2D planar geometry. The reference case considers the vehicle flying at Mach 7 and zero angle of attack at an altitude of 30 km. In this case, air compression is achieved by two ramps, one of which is the vehicle forebody itself and the other is a scramjet inlet compression ramp, and the engine cowl which satisfies the "shock-on-lip" condition. From this reference case, several other cases were simulated varying vehicle operating conditions such as altitude, velocity and angle of attack. Besides these, calculations were made for different configurations of the scramjet inlet compression geometry by varying the inlet compression ramp angle, as well as the number of inlet compression ramps. The airflow in the intake is calculated numerically with the commercial Ansys Fluent software, considering the air as a calorically perfect gas for inviscid flow. For the intake performance analysis, several parameters characterizing the intakes have been calculated and compared.

1 INTRODUCTION

The Institute for Advanced Studies (IEAv) is currently developing the 14-X Airbreathing Hypersonic Vehicle with scramjet engine propulsion, capable of flight at hypersonic speeds (M>5) at high altitudes. As part of the ongoing effort and due to a lack of significant numerical analyses of the flow conditions at flight, a number of CFD analyses have been performed using the commercial solver ANSYS Fluent.

A **scramjet** (**s**upersonic **c**ombustion **ramjet**) is a variant of a ramjet air-breathing combustion jet engine in which the combustion process takes place in supersonic airflow. As in ramjets, a scramjet relies on high vehicle speed to forcefully compress and decelerate the incoming air before combustion (hence ramjet), but whereas a ramjet decelerates the air to subsonic velocities before combustion, airflow in a scramjet is supersonic throughout the entire engine. This allows the scramjet to efficiently operate at hypersonic speeds (Mach >5):

theoretical projections place the top speed of a scramjet between Mach 12 and Mach 24, which is near orbital velocity. An airframe-integrated scramjet is basically composed of three basic components: a converging air intake, where incoming air is compressed and decelerated; a combustor, where gaseous fuel is burned with atmospheric oxygen to produce heat; and a diverging nozzle, where the heated air is accelerated to produce thrust [1, 2, 3]

This study is concerned basically with the air intake system of an airframe-integrated scramjet engine, which is consisted of the vehicle forebody, the engine inlet and the isolator duct (see Fig.1). Although many times the isolator duct, which is located between the scramjet inlet and the combustor, is not included in analyses of the compression system, here it was considered because of the interest in knowing the airflow conditions at the combustor entrance. The isolator has the main purpose of protecting the inlet from combustor high pressure effects (adverse back pressure), although, in some situations, it also contributes to the compression process. Efficient combustion of fuel requires that supersonic airflow be supplied to the combustor at suitable pressure, temperature and flow rate. In a hypersonic vehicle with scramjet propulsion it is the air intake system that has this task.

The work aims to present numerical simulations and performance analyses of a scramjet air intake configuration being tested for the 14-X scramjet engine when the vehicle operates at different flight speeds, altitudes and angles of attack. Besides, analyses have also been made for geometry deviations from the reference configuration, in terms of the number and angle of the intake ramps. For the numerical calculations, it has been considered 2D planar geometry and the calorically perfect gas and non-viscous models for the airflow. The goal is to have a better insight on the flow behavior in the air intake region of the propulsion system when changing flight parameters such as speed, angle of attack and altitude, for the reference configuration, and also to study the impact of intake geometry changes on the overall intake performance.

2 METHODOLOGY

Figure 1 presents a frame–integrated scramjet propulsion system 2D schematic. This figure shows both the main components of the system, as briefly described in the previous section, and that this geometry satisfies the “shock-on-lip” (SOL) condition at flight nominal operating conditions (Mach 7 at 30 km altitude with zero angle of attack). The SOL condition implies that the oblique shocks from the forebody and inlet ramps hit the cowl tip and reflect exactly to the top corner of the throat (red lines). [3]

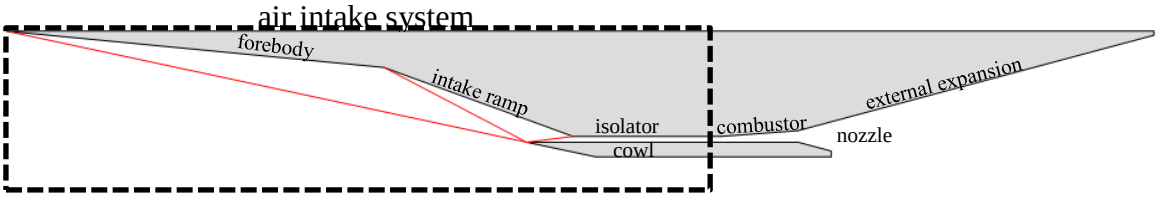

Figure 1: A frame-integrated scramjet propulsion system schematic.

2.1 Numerical calculations

The numerical simulations of the flow in the air intake region of the scramjet configurations were performed with the commercial software ANSYS Fluent using its

density-based solver which solves simultaneously the set of equations formed by the 2D inviscid flow conservation equations, Eqs. (1) through (4), the perfect gas equation of state given by Eq. (5), and others needed to close the system of equations. [4]
The continuity equation:

$$\frac{\partial \rho}{\partial t} + \nabla \cdot (\rho \vec{v}) = 0 \tag{1}$$

The momentum conservation equation in the x-direction:

$$\frac{\partial}{\partial t}(\rho \vec{v}) + \nabla \cdot (\rho u \vec{v}) = -\frac{\partial p}{\partial x} \tag{2}$$

The momentum conservation equation in the y-direction:

$$\frac{\partial}{\partial t}(\rho \vec{v}) + \nabla \cdot (\rho v \vec{v}) = --\frac{\partial p}{\partial y} \tag{3}$$

The energy conservation equation:

$$\frac{\partial}{\partial t}(\rho E) + \nabla \cdot (\vec{v}(\rho E + p)) = 0 \tag{4}$$

The perfect gas state equation:

$$\rho = \frac{p}{RT} \tag{5}$$

where ρ is the density, p is the local static pressure; T is the static temperature, R is the gas constant, $\vec{v}$ is the velocity; E is the total energy.

Figure 2 presents the geometry and computational domain of the scramjet air intake studied in this work for the reference case. The lengths are in millimeter and the main sections of the intake are also shown. The reference geometry contains two ramps: the first one is the vehicle forebody itself, and the other is a compression ramp in the scramjet inlet. Also included as part of the air intake is the isolator duct which precedes the combustor.

The mesh was created with one division per millimeter in both directions in two distinct regions, one above and the other below of the horizontal cowl line.

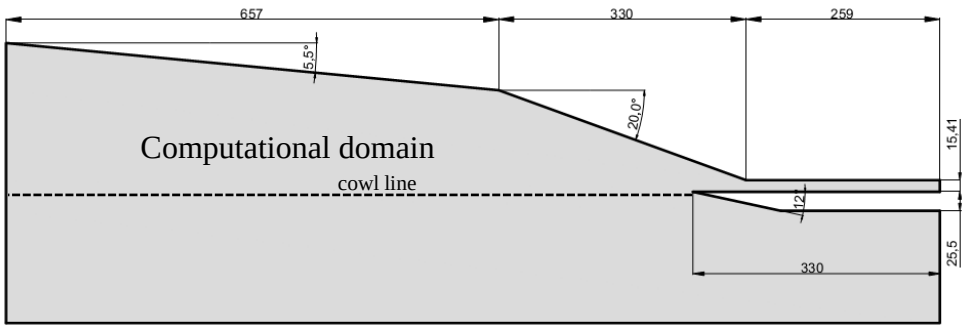

Figure 2: Reference air intake geometry

2.2 Analyzed performance parameters

Several parameters can be calculated for a scramjet air intake system in order to evaluate its performance. Some of them are simply geometric parameters and others depend on the flight operating conditions. The performance of such compression systems can be separated into parameters related to: (1) capability, or how much compression is performed, and (2) efficiency, or what level of flow losses does the intake generate during the compression process. Parameters related to the intake efficiency are important because it has an impact on the overall efficiency of the entire propulsion system. Others are concerned with the compression process and the airflow conditions entering the combustor system where combustion of the atmospheric supersonic air and the injected fuel takes place. All parameters were obtained from Smart [5] and Van Wie [4].
In order to better illustrate these parameters, Figure 3 contains a sketch of the inlet geometry containing the areas used in the calculations.

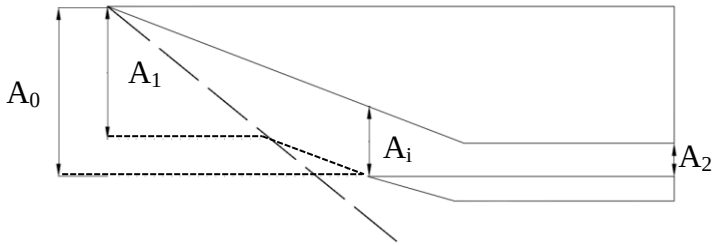

Figure 3: Scramjet inlet with its relevant areas

The contraction ratios are area ratios that directly represent the compressibility possible by the defined scramjet inlet geometry. Small contraction ratios indicate lower pressure ratios which, in turn, allow for higher velocity at the throat. An important parameter is the internal contraction ratio, which is the ratio of the cross-sectional area between the cowl lip and the compression ramp (A_i), and the throat area (A_2) which corresponds to the smallest area.

The intake air capture ratio represents the proportion of the air available for entering the engine that is really captured and flows through the isolator. It is determined by the ratio between the mass flow of air entering the engine and the available free stream one, i.e., A_1/A_0.

Parameters related to the intake compression process, such as static pressure and temperature, are also given in terms of ratios between the value of the cross-section averaged variables at the end of the isolator (combustor entrance) and the corresponding free stream ones.

Lastly, two additional parameters related to the intake efficiency are calculated. One is the kinetic energy efficiency which is defined as "the kinetic energy the compressed flow would achieve if it were expanded isentropically to free stream pressure, relative to the kinetic energy of the freestream" [5], and the other is the pressure recovery which is defined as the stagnation pressure ratio of the compression system. The latter parameter is a measure of the intake performance since total pressure losses lead to reduced axial momentum and diminish the system performance. The kinetic energy efficiency calculation is illustrated in the Mollier diagram in Figure 4.

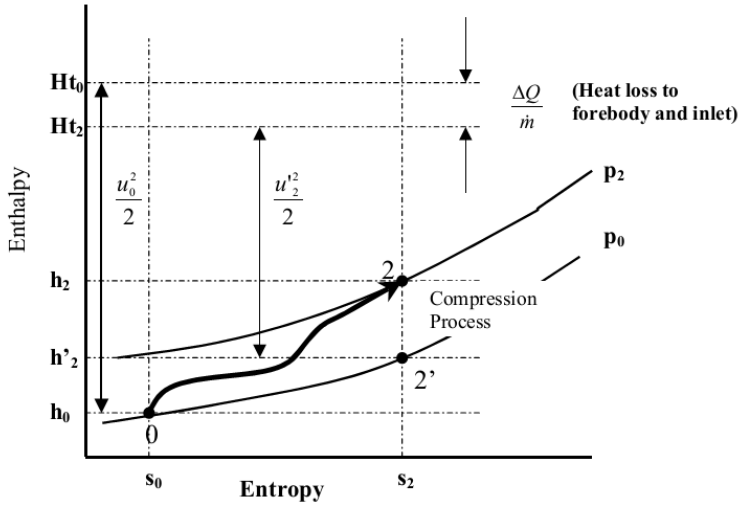

Figure 4: Kinetic energy efficiency on the Mollier diagram

Since the flow was considered as a calorically perfect gas without heat loss through the wall, the kinetic energy efficiency is the **same** as the adiabatic kinetic energy efficiency, which is calculated without considering the heat loss term in Figure 4. Therefore, for inviscid flow, these efficiencies are given by:

$$\eta_{KE} = \frac{1/2u_2^{'2}}{1/2u_0^2} = \frac{H_{t0} - h'_2}{H_{t0} - h_0} \tag{6}$$

3 RESULTS

The numerical analysis has been separated in the studies of how variations to the nominal flight conditions and to the intake geometry affect the intake airflow and the performance parameters described in the previous section.

3.1 Changes to the nominal flight conditions

In this analysis, variations to the nominal flight conditions such as vehicle speed (represented by Mach number), angle of attack and altitude are considered for the intake geometry shown in Figure 2. The nominal flight conditions consider the vehicle at Mach 7 with 0° angle of attack in an atmosphere at 30 km altitude. At these operating conditions, the shock-on-lip condition should be satisfied.

Figure 5 shows the numerically calculated Mach number contours, including a few streamlines, for the nominal conditions. Also shown in right upper corner of this figure, is a zoom of the airflow in the inlet and isolator parts of the intake. As can be seen, the shock-on-lip really occurs as the oblique shocks from the forebody and inlet ramps hit the cowl tip and reflect exactly to the top corner of the throat. This sequence of oblique shocks is responsible for the air compression process in the intake, which produces the airflow conditions at the combustor entrance. The streamlines show the changes on the flow direction in the intake caused by the shocks. Two important observations can be made from the result in this figure

due to the shock-on-lip condition: one is that the inlet captures the totality of the airflow available at the intake entrance since the shock generated in the foreboby ramp intercepts the tip of the cowl, as also indicated by the horizontal streamline which reaches the cowl tip; and the other is that the inviscid airflow is uniform in the entire region of the isolator since the reflected shock is cancelled on the throat corner, which yields uniform airflow property profiles at the combustor entrance.

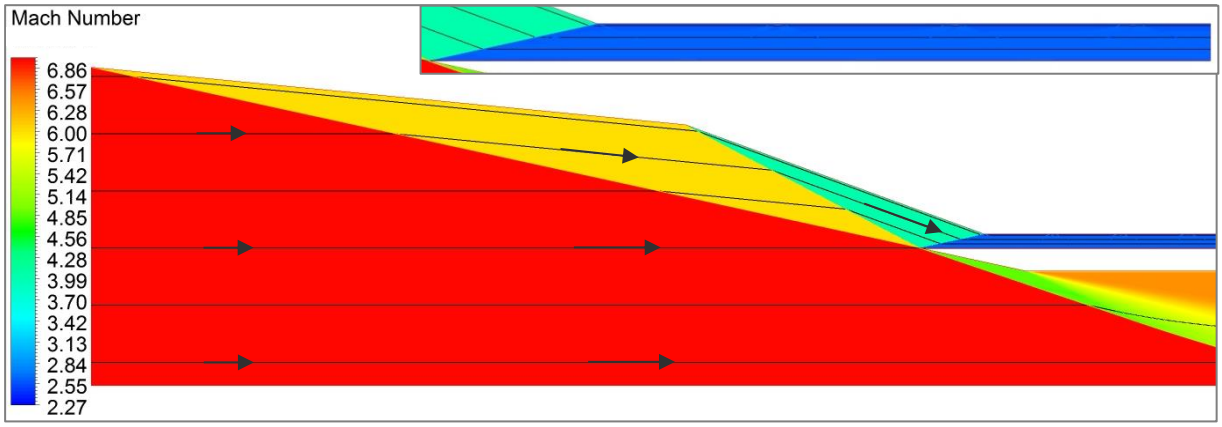

Figure 5: Mach contours and streamlines for the nominal flight conditions. Zoom of the flow inside the inlet and isolator parts of the intake.

Table 1 presents all cases analyzed considering positive and negative changes to the nominal flight operating conditions. Uncertainties of 1 Mach in the vehicle speed, 4 degree in the angle of attack and 5 km in altitude have been considered. Also, in this table, it is shown the atmospheric pressure and temperature for the corresponding altitudes.

Table 1: Flight operating conditions

Case #	Flight altitude			Mach	AOA [°]
	H [km]	P [Pa]	T [K]		
1	**30**	1,172	226.65	**7**	**0**
2	30	1,172	226.65	**8**	0
3	30	1,172	226.65	**6**	0
4	30	1,172	226.65	7	**+4**
5	30	1,172	226.65	7	**-4**
6	**25**	2,511	221.65	7	0
7	**35**	558.4	237.07	7	0

The numerical Mach contours for Mach 6 and Mach 8 cases, with respective streamlines, are presented in Figure 6: Mach contours and streamlines for (a) Mach 8 (Case 2) and (b) Mach 6 (Case 3).

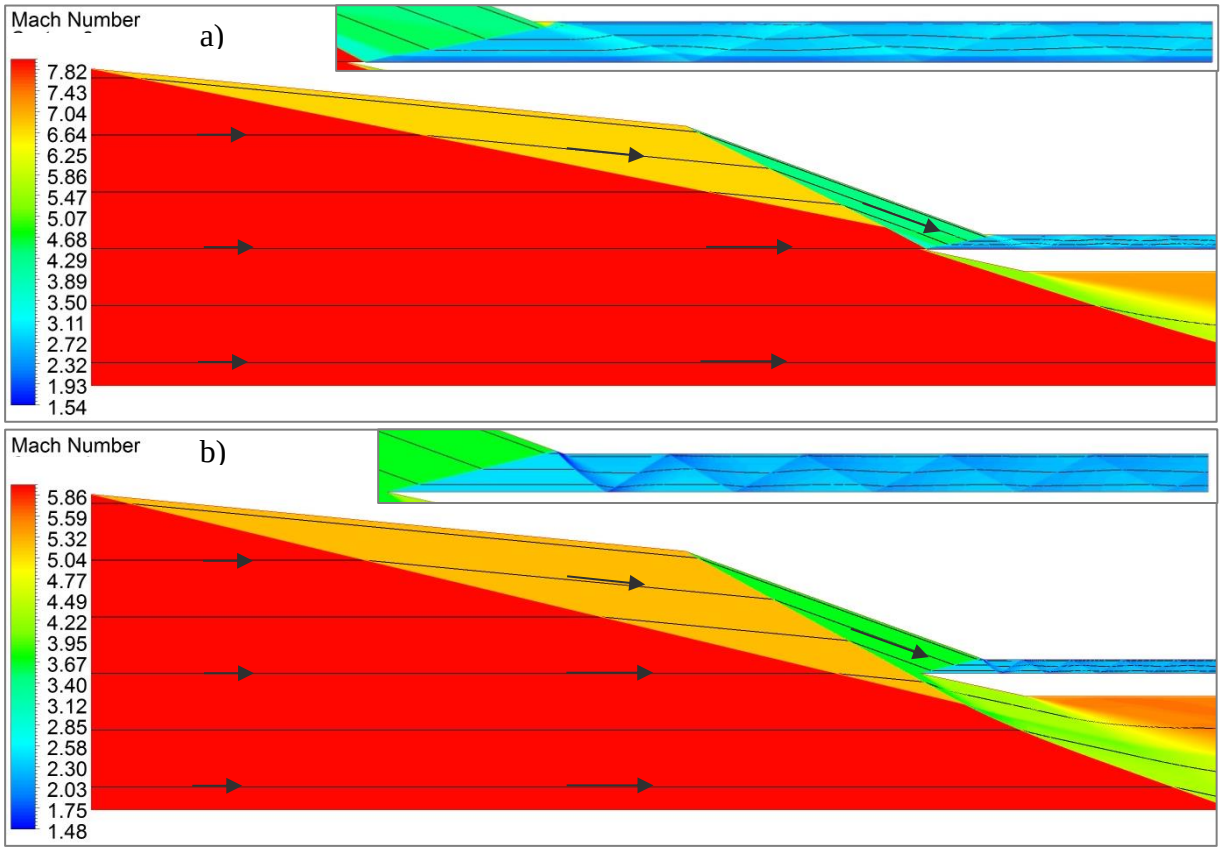

Figure 6: Mach contours and streamlines for (a) Mach 8 (Case 2) and (b) Mach 6 (Case 3).

As can be seen in Fig. 6.a, for Mach 8, a stronger shock than for Mach 7 is generated in the forebody ramp which intercepts the one generated in the inlet ramp upstream of the cowl tip and, consequently, the resulting shocks reach the cowl already inside the inlet, so the shock-on-lip condition is not satisfied. Consequently, there are additional shock compression and flow non-uniformity inside the isolator. In this case, the inlet captures the totality of the airflow available at the intake entrance since the shock generated in the foreboby ramp intercepts the inside of the cowl, as also indicated by the horizontal streamline that reaches the cowl tip. As shown in Fig. 6.b, for Mach 6, the shocks generated by the both ramps pass outside the inlet, which causes some flow spillage, i.e., part of the available airflow at the intake entrance is not captured by the inlet. The streamline that would reach the cowl tip is diverted downwards when it reaches the forebody shock, which shows that part of the available flow is not captured by the inlet. As in the case for Mach 8, the shock-on-lip condition is not satisfied, which implies also in additional shock compression and flow non-uniformities in the airflow inside the isolator.

Figure 7 presents the numerical calculation Mach contours for the cases of variations in angle of attack. In this figure, changes in the angle of attack are simulated by varying the angle of the incident free stream and keeping the angle of the intake. The angle of the streamlines at the intake entrance provides the information about the vehicle angle of attack. In Fig. 7.a, for the positive angle of attack of 4 degrees, the free stream angle with the forebody ramp increases from 5.5 to 9.5 degrees, which makes this shock stronger and, consequently, the

inlet ramp shock is weakened. The result is that these shocks intercept each other upstream of the cowl but there is still some flow spillage because the resulting shock passes outside of the cowl. Nevertheless, it is expected an increase in the inlet flow capture because the available airflow at the entrance has increased as can be observed by the streamline that would reach the cowl tip. For the negative angle of attach, as shown in Fig. 7.b, the incident angle between the free stream and forebody decreases from 5.5 to 1.5 degrees, For this situation there is still a small flow spillage and the available airflow decrease at the intake entrance as seen in this figure by the streamlines, which reduces considerably the inlet capture. In both cases, the shock-on-lip is not satisfied and, consequently, in the isolator the flow is non-uniform and there is also some additional compression.

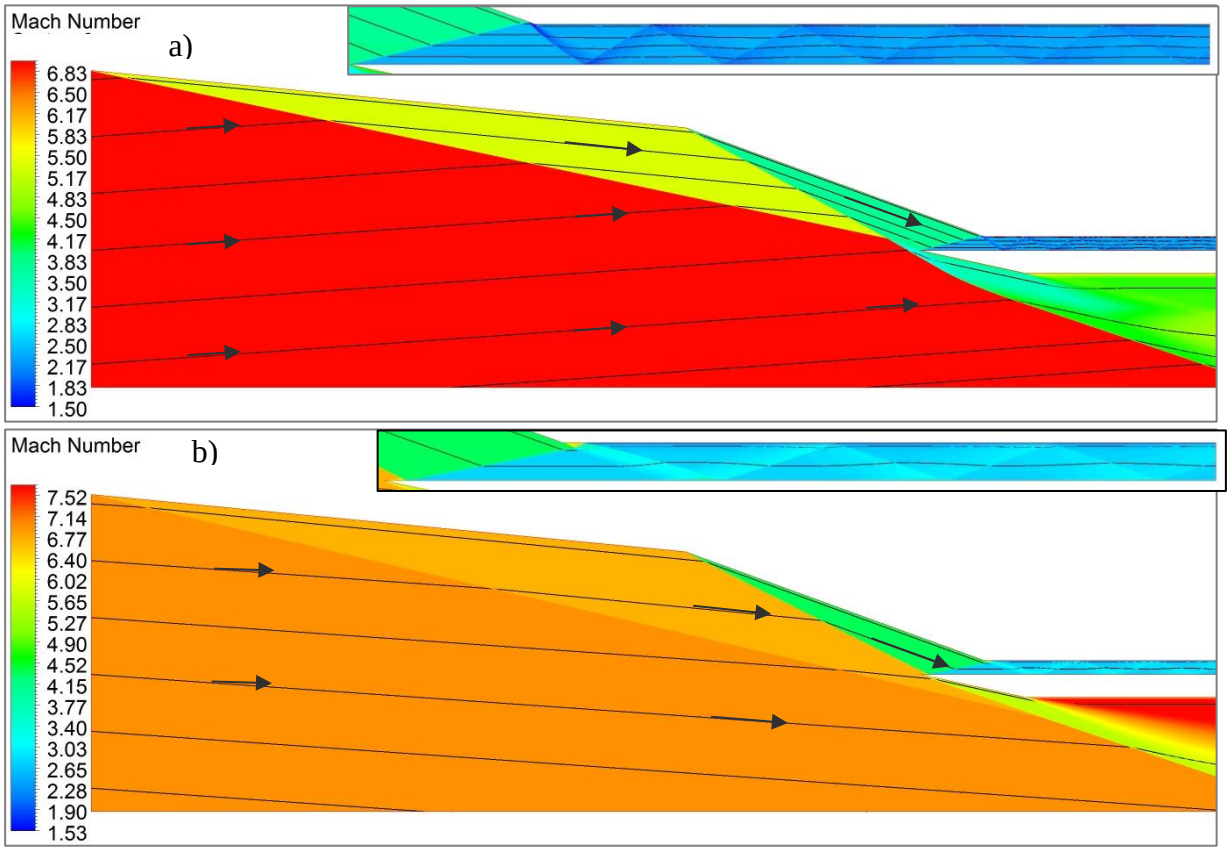

Figure 7: Mach contours and streamlines for angle of attack (a) +4° (Case 4) and, (b) -4° (Case 5).

Figure 8 shows the numerical calculated pressure profiles at the isolator exit for the cases of varying Mach number and angle of attack in comparison with the reference case. In this figure, the abrupt changes in the pressure profiles for Case 2 through Case 5 are because these cases do not satisfy the shock-on-lip condition and, consequently, the shocks entering the inlet reflects several times inside the isolator, which makes the flow properties vary significantly in this region. As expected, increasing the Mach number and the angle of attack, the compression process is more pronounced. The reference case, which obeys the shock-on-lip condition, yields basically constant profile.

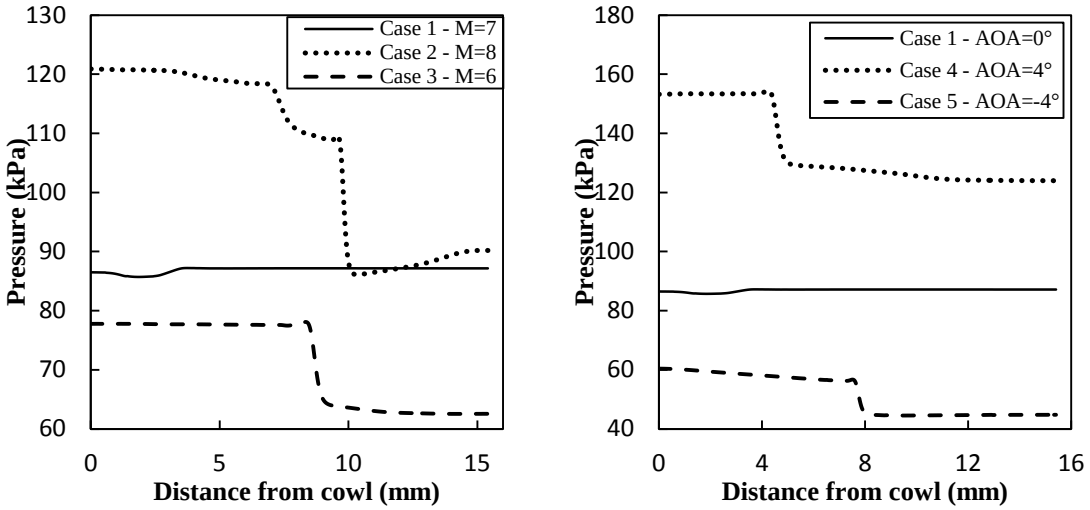

Figure 8: Pressure profiles at the isolator exit for varying (a) Mach number and (b) angle of attack.

Table 2 summarizes the calculated performance parameters and airflow properties at the isolator exit for Cases 1 to 7. The last two cases (Case-6 and Case-7) in this table refer to changes in flight altitude. For inviscid flow and calorically perfect gas models, the airflow in the intake also satisfies the shock-on-lip condition regardless of the flight altitude, so the Mach contour is the same as the one presented in Fig. 5 for the reference case. As seen in this table, the non-dimensional parameters are not modified with changes in flight altitude, although the effects on the pressure and captured mass flow are significant because of the changes in the atmospheric air properties with altitude.

The data for the efficiency parameters, pressure recovery and kinetic energy efficiency show that the latter is less affected by Mach number variation than the pressure recovery, which makes it of greater usefulness. In terms of efficiency, operation at higher Mach number and different angle of attack than the nominal values (Mach 7 and 0 angle of attack) reduce the intake efficiency while for lower Mach number the intake efficiency is somewhat increased. The compression process is more intense, generating higher pressure and temperature ratios than for the nominal conditions for higher Mach number or positive angle of attack and vice versa. Here, although the air capture ratio less than unity means that flow spillage occurs, this does not mean necessarily a reduction in the captured mass flow by the scramjet inlet because the available mass flow at the intake entrance also may vary as for Cases 2 to 5. For instance, for Cases 2 and 4, the available mass flows at intake entrance are greater than in the reference case (Case-1) and they have higher mass flow even for Case 4 which has lower than unity air capture ratio. Cases 3 and 5 present considerably lower captured mass flow than the reference case because they present not only flow spillage but also lower available mass flow at intake entrance. Airflow velocity is not much affected by angle of attack but has a more significant change with Mach number variation.

Table 2: Performance parameters and airflow properties at the isolator exit when varying flight operating conditions.

	Case 1 (M=7)	Case 2 (M=8)	Case 3 (M=6)	Case 4 (AoA +4)	Case 5 (AoA -4)	Case 6 (H=35 km)	Case 7 (H=25 km)

Total pressure recovery	0.358	0.221	0.404	0.312	0.285	0.358	0.358
Kinetic energy efficiency	0.965	0.956	0.959	0.960	0.955	0.965	0.965
Air capture ratio	1.000	1.000	0.841	0.923	0.971	1.000	1.000
Static pressure ratio	74.19	91.04	60.86	114.57	43.95	74.19	74.18
Static temperature ratio	4.580	5.655	4.177	5.388	4.230	4.580	4.579
Mass flow (kg/s.m)	7.56	8.64	5.45	9.23	5.00	16.63	3.53
Mach number	2.60	2.70	2.19	2.24	2.79	2.60	2.60
Velocity [m/s]	1681	1922	1352	1568	1727	1662	1721
Pressure [kPa]	86.9	106.7	71.3	134.3	51.5	189.1	41.6
Temperature [K]	1038	1282	947	1221	959	1015	1089

3.2 Changes to the intake geometry

This analysis intends to verify the impact of changes to the reference intake geometry (Fig. 2) on the performance parameters, presented in Subsection 2.1, and on the airflow properties at the isolator exit, for the nominal flight conditions (Mach 7, 0 angle of attack and 30 km altitude).

Here, it is considered only changes in the scramjet inlet geometry, so no changes to the vehicle forebody ramp angle is treated herein. The two first cases (Cases 8 and 9) consider changes in the angle of the inlet compression ramp of 3 degrees while the last one (Case 10) considers the scramjet inlet with two compression ramps whose angles and lengths were obtained such that the intake had the same compression ratio of the reference one (Case-1). All geometries analyzed here should satisfy the shock-on-lip condition and can be represented by the geometry in Fig. 9 with the respective lengths and angles presented in Table 3. Lengths in this table (labeled L and H) are in mm, while all angles (labeled θ) are in degree.

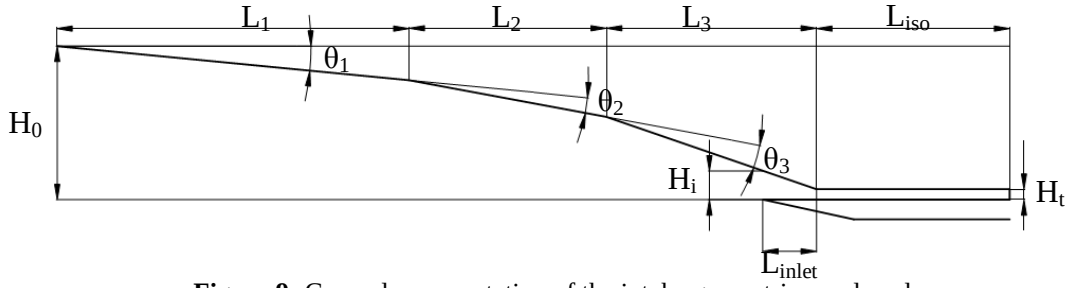

Figure 9: General representation of the intake geometries analyzed.

Table 3: Geometry data.

Case	L_1	L_2	L_3	L_{iso}	L_{inlet}	H_0	H_i	H_t	θ_1	θ_2	θ_3
1	657.34	330	-------	258.63	70.88	199.44	41.21	16.66	5.5	14.5	----
8	657.34	432	-------	258.63	99.87	213.83	49.62	19.08	5.5	11.5	----
9	657.34	260	-------	258.63	51.63	187.81	36.33	14.15	5.5	17.5	----
10	457	256	272.62	258.63	69.16	198.81	37.93	13.49	5.5	5	8.5

The flow structures in the intake for Cases 8 and 9 are similar to the reference case (Case-1), except in terms of magnitudes of the variables, because they have the same number of compression ramps and satisfy the shock-on-lip condition.

Figure 10 shows the calculated Mach contours and streamlines for the geometry with an additional compression ramp (Case-10). Since this geometry also satisfies the shock-on-lip condition, the airflow inside the isolator is uniform. It can also be seen in this figure that the change in flow direction in the region of the compression ramps is less than in the other geometries with only one compression ramp.

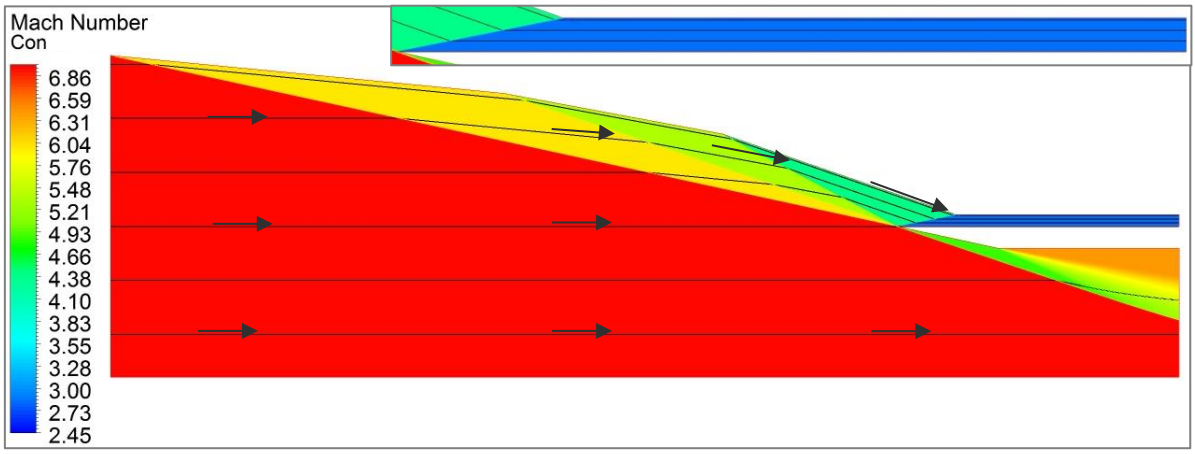

Figure 10: Mach contours and streamlines for the geometry with two compression ramps in the scramjet inlet (Case-10) for nominal flight conditions.

Table 4 summarizes the intake performance parameters and the airflow properties at the isolator exit (combustor entrance). In terms of efficiency, both Case-8 (3 degree reduction in the ramp angle) and Case-10 (two compression ramps geometry) present basically the same performance and superior to the reference case while Case-9 is considerably less efficient than the reference case. However, Case-8 yields very little compression which might not be well suitable for the combustion process whereas Case-10, which was designed to have about the same compression rate as the reference case, as can be confirmed with the data in Table 4, present not very significant variations on the Mach number, velocity and mass flow and a little bit more significant reduction on the temperature compared to the reference case. All geometries presented not much different internal contraction ratios, although the Case-10 is the one which has the highest value.

Table 4: Performance parameters and airflow properties at the isolator exit for different intake geometries at nominal flight conditions.

	Case 1	Case 8	Case 9	Case 10
Total pressure recovery	0.358	0.472	0.263	0.507
Kinetic energy efficiency	0.965	0.976	0.953	0.978
Internal contraction ratio	4.82	4.32	5.21	5.33
Air capture ratio	1.000	1.000	1.000	1.000
Static pressure ratio	74.19	50.37	101.53	73.63
Static temperature ratio	4.580	3.787	5.470	4.136
Mass flow (kg/s.m)	7.56	8.16	7.10	7.56
Mach number	2.60	3.04	2.21	2.84
Velocity [m/s]	1681	1785	1556	1740

Pressure [kPa]	86.9	59.0	119.0	86.3
Temperature [K]	1038	858	1240	937

4 COMMENTS AND CONCLUSION

It has been presented numerical and performance analyses of the air intake region of the scramjet propulsion system being presently tested for the 14-X hypersonic vehicle prototype. This study had the main purpose of giving information on how the efficiency, mass capture and the compression process of the intake system are modified for flight operating conditions which differ from the nominal ones as well as for some changes in the reference geometry. At this stage of the numerical studies, the model was based on the assumptions of 2D geometry, calorically perfect gas and inviscid airflow, which is still capable of providing relevant information on the intake system compression capability and on the losses related to the non-isentropic process that exists in this region. The analysis showed how off-design operation, such as Mach number and angle of attack, modifies the flow structure and affects mass capture and airflow condition entering the combustor. Also, the two inlet compression ramp geometry yielded basically the same mass capture and compression capability as the reference geometry with even higher efficiency, so this geometry should also be considered for future analysis.

Although the present modeling is useful for providing a first insight on the intake performance, some phenomena which might alter significantly the airflow in the intake from the one calculated with this modeling, can only be studied with more realistic models which consider, for instance, viscous flow, non-adiabatic walls, 3D geometry, high temperature effects, and so on. Therefore, future work on the air intake of the scramjet propulsion system for the 14-X vehicle should certainly consider such models.

5 ACKNOWLEDGMENTS

This work has been performed with CNPq/AEB financial support under the Project number 560143/2010-9.

6 REFERENCES

[1] Smart, M., 2008, Scramjets. In *RTO-EN-AVT-150 Lecture Series.* Rhode St. Genèse, Belgium.

[2] Segal, C., 2009, *The Scramjet Engine: Processes and Characteristics.* Cambrigde University Press, New York.

[3] Van Wie, D.M., 2000, Scramjet Inlets, in: *Scramjet Propulsion*, Edited by E.T. Curran and S.N.B. Murthy,
Progress in Astronautics and Aeronautics, Vol. 189, American Institute of Aeronautics and Astronautics,
Inc., Reston, VA, Chapter 7, pp. 447-511.

[4] Anderson, J.D., 1995, *Computational Fluid Dynamics.* McGraw-Hill, New York.

[5] Smart, M., 2010, Scramjet Inlets. In *RTO-EN-AVT-185 Lecture Series.* Rhode St. Genèse, Belgium.